Review Article

International Journal of Chemistry and Aquatic Sciences (IJCA)
Vol.12.Issue.1.2026(Jan-March), Page: 1-29
ISSN: 2355-033X
http://chemistryjournal.kypublications.com/

Comprehensive Review of Conventional Adsorbents and Biopolymer Nanocomposites for Fluoride Removal and Future Research Directions

Paul M. Munene[1], Nthiga E. W.[2]
[1]*Department of Biological & Physical Sciences, Turkana University College, Kenya*
[2]*Department of Chemistry, Dedan Kimathi University of Technology, Kenya*
Corresponding Author: Paul M. Munene
Email: pmunene@tuc.ac.ke
doi: 10.33329/ijca.12.1.1

Article info
Article Received:16/01/2026
Article Accepted:20/02/2026
Published online:25/02/2026

ABSTRACT
Groundwater pollution with fluoride is a global health concern affecting over 200 million people. Fluoride enrichment of groundwater is mainly accelerated by subsurface leaching causing adverse health effects such as skeletal fluorosis when fluoride levels exceed 1.5 mg/L. In an attempt to offer a lasting solution on fluoride removal, researchers have developed as well as modified diverse adsorbents. Biopolymer adsorbents such as chitosan have attracted growing attention due to biodegradability, lower cost, biocompatibility, regenerability, high number of activatable functional groups and high efficiency depending on activation methods. The emerging nanotechnology has enabled synthesis of biopolymer nanocomposites that have exhibited enhanced physical, chemical, electrical and thermal capabilities leading to higher removal efficiency. Crosslinking modification of biopolymer is reported to further enhance mechanical strength and ease of recovery thus preventing secondary pollution. Diverse characterization technologies have evolved for better understanding of surface morphology, chemical composition and crystal structure, thermostability, surface area, zeta potential, molar mass distribution and crosslinking success of biopolymer nanocomposites. Future research should focus on applying safe activation methods, enhancing porosity, safety, efficiency, stability, mechanical strength and selectivity in biopolymer nanocomposite fabrication.
Key Words: Defluoridation, Crosslinking, Nanocomposites, Efficiency and Safety

1. Introduction

Water is a vital component for life and a universal solvent (Robayo-Amortegui *et al., 2024*). However, safe water is scarce for purposes such as drinking, agriculture and industrial production among others (Abanyie *et al.*, 2023). Recent research has focused on remediation of toxic water contaminants such as fluoride in both surface and groundwater for sustainable healthy living.

Fluorine exists in nature as a complex or in its ionized form, fluoride (F^-) whose high electronegativity influences its occurrence and reactivity in nature (Johnston & Strobel, 2020).

Fluoride levels below World Health Organization's limit of 1.5 mg/L are considered a micronutrient that prevents dental caries through mineralization while long-term exposure to higher levels not only causes dental and skeletal fluorosis but also adverse cardiovascular, neurological, reproductive, genetic and endocrine effects (Akafu *et al*., 2019; Santhi *et al*., 2024).

Untreated wastewater from anthropogenic activities such as glass and ceramic industries may increase fluoride levels in groundwater (Sarma *et al*., 2020). However, subsurface leaching from bedrock minerals such as fluorspar and fluorapatite has been reported as the prime source of fluoride enrichment (Akafu *et al*., 2019). Fluoride pollution is a worldwide problem affecting approximately 200 million people in both developed and developing countries such as USA, India, China and Kenya among others (Nocella *et al*., 2022). In Kenya, the problem is widespread in the Rift Valley region where research reported noncomplying fluoride levels of 5.87 mg/L in borehole water from Turkana County located in Kenyan Northern Rift region (Rusiniak *et al*., 2021).

Substantial researches have documented defluoridation as the practical solution to fluoride problem in drinking water. The existing defluoridation technologies include ion exchange which is selective and efficient but strongly influenced by coexisting anions such as sulphates, carbonates and phosphates (Grzegorzek *et al*., 2020; Sun *et al*., 2023); membrane processes such electrodialysis, reverse osmosis and nanofiltration which are efficient but limited by high energy consumption and cost for the ion-exchange membranes (Sun *et al*., 2023); coagulation which is limited by high coagulant cost, lower efficiency caused by precipitates and secondary water pollution (Sun *et al*., 2023).

Electrocoagulation enhances efficiency but is limited by scale formation and high energy costs (Grzegorzek *et al*., 2020) and adsorption process which is considered superior to all conventional methods due to its efficiency, simplicity, safety, regenerability and low cost among other advantages (Garba *et al*., 2019; Hgde *et al*., 2020; Tazik *et al*., 2023). Due to this, adsorption process is accessible by rural communities depending on fluoridated groundwater in developing countries.

The effectiveness of an adsorbent depends on its physical and chemical properties such as pore volume, specific surface area (S_{BET}), point of zero charge (pH_{PZC}), surface chemistry, mechanical and chemical stability; the features of the adsorbate such as chemical speciation, thermodynamic state and factors such as pH, contact time, temperature, initial adsorbate concentration and competitive coexisting ions (Othmani *et al*., 2023).

In the recent years, researchers have developed diverse adsorbents such as metal oxide/hydroxide which are efficient especially when modified but limited by cost of loaded metals (Wei *et al*., 2022) and secondary pollution (Yu *et al*., 2024); carbon based adsorbents which are efficient but limited by high pyrolysis energy (Senewirathna *et al*., 2022) and secondary pollution by loaded metals and aluminosilicate adsorbents limited by secondary pollution (Wei *et al*., 2022).

Biopolymer composites such as chitosan composites have attracted growing attention due to non-toxicity, low cost, regenerability, low leaching, biodegradability, biocompatibility and hydrophilicity (Valdez-Alegria *et al*., 2020; Žigrayová *et al*., 2024), and enhanced efficiency when successfully modified using non-toxic methods. Crosslinking modification of biopolymers using appropriate crosslinkers enhances their pore volume, mechanical, chemical and thermal properties besides solving recovery challenges (Valdez-Alegria *et al*., 2020). Activation of functional groups such amino ($–NH_2$) and hydroxyl (-OH) groups enhances affinity for fluoride fostering higher removal efficiency (Žigrayová *et al*., 2024). Fabrication of biopolymer nanocomposites enhances surface area and removal efficiency (Sarma *et al*., 2020), selectivity, physical, chemical and thermal stability.

This current review aims at providing insights on gaps in conventional adsorbents and synthesis of biopolymer nanocomposites; activation methods, crosslinking and characterization and future perspectives.

2. Conventional Adsorbents

2.1 Metal Oxide/Hydroxide Adsorbents: Metal oxides/hydroxides based on iron (Mashale *et al*., 2025), aluminum (Gai & Deng, 2021), zirconium (Zhao *et al*., 2024) and lanthanum (Li *et al*., 2022) are among the effective adsorbents because their surfaces contain metal-hydroxyl (M-OH) groups that can interact strongly with various contaminants in water. Their primary adsorption mechanisms are ligand exchange for pollutants such as oxyanions (like phosphate, arsenate, and fluoride) and electrostatic interactions for anions and cations with respect to pH of the point of zero charge (PHpzc). For pH value < PZC of the adsorbent, the adsorbent is protonated, hence positively charged. In this case, F^- adsorption is attributed to the electrostatic attraction between F^- and the adsorbent (Gai & Deng, 2021).

$$AlOOHH^+ + F^- \rightarrow AlOOHHF \quad (1)$$

Addition of a metal oxide or hydroxide adsorbents into an aqueous solution results in formation of a layer of hydroxyl groups on the surfaces of the adsorbent through a hydration reaction. If the metal has a stronger affinity for fluoride than the hydroxyl group, a ligand exchange reaction between F^- and the hydroxyl group occurs.

$$F^- + \equiv MOH \leftrightarrow \equiv MF + OH^- \quad (2)$$

Nano-structured metal oxide/hydroxide adsorbents are currently attractive to researchers due to enhanced adsorption capacity promoted by favorable surface area and quantum properties.

2.1.1 Aluminium Oxide/Hydroxide: Aluminium hydroxide is first synthesized by electrolysis or pyrolysis and then partially converted to aluminum oxide by calcination. High adsorption efficiency in aluminum oxide/hydroxide is due to large specific surface area and reactivity. The mechanisms of fluoride removal by aluminium hydroxide are electrostatic attraction and ion exchange. Liu *et al*., 2011 synthesized amorphous aluminium hydroxide ($Al_2O_3.\ xH_2O$) through enhanced hydrolysis with S_{BET} = 118.24 m^2/g, Q_{max} of 128.0 mg/g and adsorption mechanisms proposed as chemisorption and ion exchange. The high adsorption capacity was attributed to low particle size, high surface area and favorable zeta potential. Similar studies by Dhawane *et al*. (2017) using thermally activated alumina (Al_2O_3) reported a maximum fluoride removal of 86.1% attributed to high surface area of 185.6 m^2/g and pore volume of 0.2351 cm^3/g.

The adsorption mechanism was both physical and chemical. The study found activated alumina to be a prominent adsorbent for fluoride removal. However, aluminium ions may leach into treated water degrading its quality.

2.1.2 Magnesium Oxide (MgO)/MgO Composites: MgO has been confirmed as an attractive adsorbent due to its high adsorption capacity, non-toxic nature and limited solubility in water. Devi *et al*. (2014) studied nano-magnesium oxide adsorbent and reported maximum fluoride removal of 90% attributed to high surface area, S_{BET} of 92.46 m^2/g and pore volume of 0.4313 mL/g, isomorphic substitution of –OH by F^- and multilayer adsorption. The setback of secondary contamination as a result of leaching also applies to magnesium oxide adsorbents. In an attempt to address the secondary pollution, losses and recovery challenges with MgO adsorbent, Yu *et al*. (2024) reported MgO/Rice husk biochar and MgO/spent coffee biochar composite adsorbents with enhanced removal of 80% and 86%, respectively.

2.1.3 Layered Double Hydroxides (LDH): Coupled adsorbents combine the quantum coupling and synergistic effects of individual metal cations resulting even in tripling of adsorption capacity (Wei *et al*., 2022).

LDH have the formula $[M_x^{2+}M_{1-x}^{3+}(OH_2)]^{x+}(A^{n-})_{\frac{x}{n}}.mH_2O]$ where, M^{2+} is the positive divalent metal ion such as Mg^{2+}, M^{3+} is the positive trivalent metal ion such as Al^{3+} and A is the negative interlayer anion such as Cl^-. The LDH lamella has replaceable metal hosts and exchangeable anions, increasing affinity for fluoride (Cai *et al*., 2018; Wei *et al*., 2022). Current research shows that doping the LDH with a rare earth element such as La^{3+} further increases the adsorption capacity. In that context, Cai *et al*. (2018) reported a La doped Li/Al LDH with Q_{max} of 35.4 mg/g.

2.1.4 Rare Earth Metal Oxides: Rare earth metals such as lanthanum, cerium and titanium have high affinity for fluoride due to the ability to stabilize in the +3 or +4 valence state with a few numbers of outermost electrons; therefore, empty orbitals are available for fluoride removal (Wei *et al*., 2022). The oxides of the rare earth metals have been studied for synthesis of highly efficient fluoride adsorbents.

For instance, CeO_2 has attracted attention due to oxygen vacancy formation hence high oxygen storage, release capacity and adsorption capacity (Kang *et al*., 2017). Kang *et al.* (2017) found adsorption performance to be dependent on three different morphologies of CeO_2 with CeO_2-nanorods recording the highest Q_{max} at 71.5 mg/g while CeO_2-octahedrons and CeO_2-nanocubes having 28.3 and 7.0 mg/g, respectively. The three materials exposed different active sites as indicated by their different specific surface areas and pore volumes with CeO_2-Octahedrons showing the largest specific surface area and pore volume (160.2 m^2 /g, 0.387 cm^3 /g), followed by the CeO_2-nanorods (111.4 m^2 /g, 0.241 cm^3 /g) and CeO_2-nanocubes (55.8 m^2 /g, 0.211 cm^3 /g). The fluoride removal mechanisms proposed for the three materials were Ce^{3+}-O defects, ion exchange, surface adsorption and pore filling. In depth research also shows that lanthanum-based adsorbents are highly effective due to strong affinity, high selectivity and environmental safety (Yang *et al*., 2022). Such an adsorbent was lanthanum methanoate adsorbent synthesized by amide-hydrolysis which recorded Q_{max} of 268.99 mg/g (Yang *et al*., 2022). To date, the scaling up of rare earth metals adsorbents is limited by high cost, agglomeration, coexisting ions and leaching (Wei *et al*., 2022).

2.2 Carbon Based Adsorbents

2.2.1 Activated Carbon/Base and Acid Modified Activated Carbon/Activated Carbon Composite/Metal doped Activated Carbon: Activated carbon is obtained from coal, wood and coconut shells among other raw materials (Wei *et al*., 2022). The high adsorption capacity in activated carbon can be attributed to large surface area and porosity. To synthesize activated carbon, the crushed and dehydrated material is carbonized by heating in anaerobic conditions at high pyrolysis temperature (500-900˚C). The adsorbent is further activated using acids, bases or salts (Senewirathna *et al*., 2022). The functional groups such as hydroxyl, carboxyl and amine on the surface of the biomass adsorbent are involved in fluoride removal. KOH activated carbon by Araga *et al*. (2017) yielded a high surface area, S_{BET} of 747.45 m^2 g^{-1}, pore volume of 0.41 cm^3 g^{-1} and Q_{max}= 3.65 mg g^{-1}.

Similarly, phosphoric acid activated carbon by Senewirathna *et al*. (2022) recorded 61.0% adsorption efficiency. Activated carbon composites have been reported to have synergistically higher fluoride removal capacity. Tolkou *et al*. (2024) reported chitosan/orange peels/activated carbon@MgO composite with 97% fluoride removal efficiency. Iwar *et al*. (2022) reported an activated carbon/aluminium oxide composite with removal efficiency of 99.1%. Similarly, metal doping of activated carbon with rare earth metals showed enhanced efficiency as reported by Kim *et al*. (2020).

2.2.2 Bone char/Metal-doped Bone char: Bone char is the charring product of animal bones and generally contains about 70–76% hydroxyapatite (HAP), 7–9% calcium carbonate and 9–11% amorphous carbon (Alkurdi *et al*., 2019; Wei *et al*., 2022), with the percentage of each varying with the degree of charring temperature. Previous research indicated 500-700˚C as the optimal charring temperature beyond which surface area and pore volume are reduced lowering fluoride removal efficiency (Alkurdi *et al*., 2019).

Raising temperature above the optimum causes dihydroxylation of HAP adversely altering its structure (Patel *et al*., 2015). Similarly, lowering the temperature below 500 °C will result in contamination of water with organic matter due to the incomplete removal of organic matter in the bone structure. Patel *et al*. (2015) examined the effect of charring temperature and residence time reporting the highest surface area of 114.149 m^2/g, pore volume of 0.294 cm^3/g and mesoporous structure at 400˚C and time 2 hours.

Hydroxyapatite has been reported to be responsible for fluoride removal when –OH groups are replaced by F^- as expressed by equation (3):

$$Ca_{10}(PO_4)_6OH + 2F^- \rightarrow Ca_{10}(PO_4)_6F_2 + 2OH^- \quad (3)$$

The mechanisms involved in fluoride removal are ion exchange, precipitation and electrostatic interaction. Introduction of trivalent metal cations such as Fe^{3+} and Al^{3+} to the bone char enhances affinity to the highly electronegative fluoride. Aluminium impregnation of bone char by Rojas-Mayorga *et al*., 2015 enhanced fluoride removal up to 600%.

This was superior to iron doped bone char in the same experiment. Metal modification enhances adsorption capacity of bone char. In connection to this, Zuniga-Muro *et al*. (2017) doped bone char with Ce^{4+} achieving Q_{max} of 13.6 mg/g and antibacterial properties.

2.2.3 Biochar/Acid Modified Biochar/Metal Doped Biochar: Biochar is made from waste biomass materials such as bagasse, tea and rice husk (Girkar *et al*., 2024). Biochar is carbon-rich, fine-grained, porous, and highly aromatized material for application as adsorbent. Facile synthesized biochar by pyrolysis is effective but not as activated biochar. Goswami & Kumar (2018) achieved removal efficiency of 90% and Q_{max} of 21.7 mg/g using pyrolysed biochar.

In examining acid and hydroxide modified biochars, Aboulsoud (2024) discovered higher surface area of 85.61±0.02 m^2/g, pore volume of 0.086±0.001 cm^3/g and Q_{max} of 109.18 mg/g in acid modified biochar. The acid modified biochar showed more active functional groups such as –OH, -COOH and –C=O favorable for adsorption. Aluminium hydroxide has high pH_{PZC} hence $Al(OH)_3$ loaded biochar has demonstrated the ability to adsorb fluoride in alkaline pH range. Doping with rare earth metals such as La further synergistically improves fluoride removal capacity. Metal modified La/Fe/Al-rice straw by Zhou *et al.* (2021) indicated hydroxyl and positive sites formation greatly enhancing adsorption capacity, resistance to pH changes and coexisting ions.

2.3 Natural Mineral Clays such as Zeolite/Zeolite Composites: Zeolite, a microporous aluminosilicate has high potential to adsorb fluoride due to large surface area (Wei *et al*., 2022). Zeolite has been incorporated as support in other adsorbents with poor mechanical properties providing synergistic adsorption effects in the process. Chitosan/Zeolite composite was reported by Arcibar-Orozco *et al.* (2020) with removal of 70%, best at lower chitosan concentration. Metal modified zeolite was reported to have higher synergistic removal of 80% by Yang *et al*. (2021).

2.4 Biopolymer Adsorbents: Biopolymers are natural macromolecular materials with properties such as biodegradability, nontoxicity, low waste generation, low leaching, biocompatibility and hydrophilicity (Valdez-Alegria *et al*., 2020). Extensive research has gone to chitosan, sodium alginate, pectin and carboxymethylcellulose (Wei *et al*., 2022). Hydrogels produced by physical and chemical crosslinking have improved pore size, chemical, mechanical and thermal resistance making them superior adsorbents (Valdez-Alegria *et al*., 2020). The composites of biopolymers with materials like bentonite and montmorillonite among others have attracted attention of researchers due to enhanced adsorption capacity.

2.4.1 Sodium Alginate/Metal-doped Alginate: Sodium alginate is a natural anionic polysaccharide with large number of –OH and –COOH extracted from brown algae or bacteria. It is a promising material for fluoride ion removal through ion exchange interaction due to its abundant resources, high bio-compatibility, low cost, and the presence of abundant hydroxyl groups (Chang *et al*., 2024). During ionic crosslinking of sodium alginate, high-valent metal cations (Ca^{2+}, Ce^{3+}, Fe^{3+}, Al^{3+}, La^{3+} etc.) rapidly replaces Na^{+} in forming ligand chelate crosslinks with the oxygen atoms in the carboxyl and hydroxyl groups of the G-units, which form irreversible hydrogel-like microbeads (Wei *et al.,* 2022) improving fluoride removal. Chang *et al*., 2024 fabricated aluminium alginate foam with enhanced surface area of 22.24 m^2/g and Q_{max} of 7.56 mg/g.

2.4.2 Chitosan/Chitosan Composites/Metal-doped Chitosan: Chitosan is a polycationic (Nagaraj & Kumar, 2018), non-toxic, biodegradable, biocompatible biopolymer extracted from exoskeletons of crustaceans, mollusks, insects and cell walls of fungi through deacetylation process (Pathak *et al*., 2021). The biopolymer has drawn attention due to large number of modifiable amino and hydroxyl functional groups for fluoride removal. Nagaraj & Kumar (2018) found that powder chitosan had higher removal efficiency of 71.17% compared to solution chitosan having 66-70%. Substantial research has shown chitosan nanocomposites to have higher surface area and pore volume for fluoride removal. Li *et al*., 2022 reported increment in the surface area and pore volume of chitosan modified activated sludge lysis ash from 26.91 to 57.46 m^2/g and 0.081 to 0.113 cm^3/g, respectively.

Metal impregnated chitosan has shown enhanced adsorption capacity and resistance to pH changes. Sarma *et al*., 2020 synthesized an efficient Zn-Fe-Ch nanocomposite whose surface area and pore volume increased significantly from 5.523 to 73.235 m^2/g and 0.014 to 0.143 cm^3/g, respectively.

2.4.3 Gelatin/Gelatin Composites/Metal-doped Gelatin: Gelatin is a naturally occurring high molecular weight polypeptide extracted through partial hydrolysis from various animal waste bone and skin such as pigs, cattle and fish (Rather *et al*., 2022). It is non-toxic, amphoteric, biodegradable, biocompatible, unsolvable in organic solvents but solvable in glycerol, hot water and acetic acid. Gelatin is a very effective adsorbent due to the polymorphism structure of its functional amino acid group and carboxyl acid groups (Sultana *et al*., 2023). Literature review showed scanty research involving stand-alone gelatin adsorbents for fluoride removal. However, gelatin composites yielded impressive synergistic performance. Metal doping of gelatin enhances fluoride affinity and removal performance. The impregnation of cross-linked gelatin with La^{3+} in a study by Zhou *et al.* (2004) yielded 98.8% removal. Zirconium-based metal-organic frameworks (MOFs) integrated with gelatin aerogels have shown enhanced capacities for removing fluoride ions across a wide pH range (Kim *et al*., 2025). Table 1 presents a summary of previous research on biopolymer composites.

Table 1: Summary of modification method, characteristics, adsorption capacity and adsorption mechanisms of gelatin and chitosan biopolymer composites.

Adsorbent	Modification method	S_{BET} (m^2/g)	Pore Volume (cm^3/g)	PH_{PZC}	Q_{max} (mg/g)	Adsorption mechanism	Isotherm	Reference
Zeolite/chitosan composite	Mixing chitosan solution in acetic acid with zeolite solution in deionized water	7.0	0.03	8.7	5.44	Electrostatic attraction, ion exchange	Langmuir	Arcibar-Orozco *et al.,* 2018

Activated sludge lysis ash/chitosan (ASLA/C) composite	Co-precipitation	57.46	0.113	-	7.714	Electrostatic adsorption, ion exchange, surface complexation and hydrogen bonding	Langmuir	Li *et al.*, 2022
Chitosan/Orange Peels/Activated Carbon@MgO	Mixing and crosslinking	-	-	8.95	26.92	Chemisorption, electrostatic attraction and hydrogen bonding	Langmuir	Tolkou *et al.*, 2024
Chitosan modified Zn/$ZnFe_2O_4$ nanocomposite	Co-precipitation coupled with hydrothermal aging	73.235	0.143	-	-	Electrostatic attraction	Freundlich	Sarma *et al.*, 2020
Hydroxyapatite /gelatin nanocomposite	Co-precipitation	80.0	0.3	-	-	Ion exchange	Langmuir	Fernando *et al.*, 2021

3. Emerging Nano scale Technology

For a long time, conventional adsorbents have been applied in defluoridation of drinking water but are limited by setbacks including low efficiency, limited adsorption capacity, recovery challenges, high energy consumption, expensive raw materials and poor mechanical and chemical properties. In recent years, researchers have innovated considerably efficient adsorbents through modifications such as metallic doping and nanocomposites (Sarma *et al*., 2020).

Nanotechnology involves manipulating the size of materials to size of 1-100 nm yielding enhanced physical, chemical, electrical, and thermal capabilities (Panhwar *et al*., 2023).

Nanotechnology has been widely applied in medicine and electronics compared to water treatment but recently has attracted growing attention due to enormous potential in water treatment and environmental protection (Panhwar *et al*., 2023). Nano adsorbents have exhibited high surface area and removal efficiency (Sarma *et al*., 2020), selectivity, physical, chemical and thermal stability. Magnetic nanoparticles have been reported to have ease of separation at the recovery stage, lowering risk of secondary pollution (Panhwar *et al*., 2023). Magnetic nanoparticles have been fabricated through co-precipitation (Sarma *et al*., 2020), hydrothermal, solvochemical and ultrasonic activation among others (Jaldurgam *et al*., 2021). These methods are also used to prepare the 1D and 2D nanostructures such as nanoflakes, nanotubes and nanorods (Jaldurgam *et al*., 2021).

4. Biopolymer Activation Methods

Due to the setbacks with conventional adsorbents such as limited adsorption capacity, high cost and risk of secondary pollution, researchers have explored new cost effective and safe adsorbents. Biopolymers such as chitosan and gelatin have attracted much attention due to non-toxicity, biodegradability, biocompatibility and presence of activatable functional groups such as $–NH_2$ and -OH (Miretzky & Cirelli 2011). For instance, the $–NH_2$ groups are protonated in acidic media becoming active sites for adsorption of fluoride through electrostatic attraction (Miretzky & Cirelli 2011). Due to chitosan having low mechanical strength and difficult separation from solution after adsorption (Huang *et al*., 2012), crosslinking is done using a suitable crosslinker that doesn't have antagonistic effects on fluoride removal.

Current research has also reported chitosan supports such as Fe_2O_3 resulting in composites with higher removal capacity. Flake and powder forms of chitosan are not suitable for use as adsorbents due to their low surface area and no porosity hence are modified into beads to enhance adsorption performance (Miretzky & Cirelli 2011). Chemical modification of chitosan is of interest since it doesn't change the skeleton structure but leads to new derivatives with improved properties for specific application. The new functional groups are incorporated to increase the density of sorption sites, change the pH range for fluoride adsorption and change the sorption sites in order to increase sorption selectivity for the target adsorbate (Miretzky & Cirelli 2011).

4.1 Protonation of $-NH_2$ group to N^+H_3: The NH_2 is protonated in acidic media to N^+H_3 and removal of fluoride is due to electrostatic attraction between negatively charged fluorides and positively charged N^+H_3. Huang *et al*., 2012 reported protonated cross-linked chitosan particles with results presented in table 2.

Table 2: Summary of protonation method of biopolymer adsorbents

Adsorbent Material	Q_{max} (mg/g)	Optimal pH	Isotherm Model	Kinetic Model	Thermody-namics	Mechanism Proposed	Adsorbent Characterization	Reference
Protonated cross-linked chitosan particles	8.10	7	Langmuir and Freundlich	-	-	Electrostatic attraction	FTIR, XRD and SEM	Huang *et al*., 2012

4.2 Carboxylation of $-OH$ group to $-OCH_2COOH$: Chitosan beads are treated with aqueous 0.5 M chloroacetic acid maintained at pH 8.0 using 0.1 M NaOH for 10 h at room temperature to convert the hydroxyl groups to carboxyl groups. The acidic hydrogen (–COOH) is bonded to the F^- electrostatically and via hydrogen bonding which suggests fluoride removal is by means of electrostatic adsorption and Lewis acid–base interaction (Viswanathan *et al*., 2009). Viswanathan *et al*. (2009) reported carboxylated chitosan for fluoride removal as presented in table 3.

Table 3: Summary of carboxylation method of biopolymer adsorbents

Adsorbent Material	Q_{max} (mg/g)	Optimal pH	Isotherm Model	Kinetic Model	Thermody-namics	Mechanism Proposed	Adsorbent Characterization	Reference
Carboxyl at-ed crosslinked chitosan beads	1385	7	Langmuir and freundlich	Pseudo second-order	Spontaneousand endothermic	Electrostatic adsorption and Lewis acid–base interaction	FTIR and SEM with EDAX	Viswanathan *et al*., 2009

4.3 Incorporation of Electropositive Multivalent Metals to Chitosan Beads: Due to high electronegativity and small radius, F^- has strong affinity for electropositive multivalent metal cations such as La^{3+}, Fe^{3+}, Ce^{3+} and Al^{3+}. These metal cations complete their coordination shells with -OH groups that can bind or release H^+ depending on the solution pH. Under acidic conditions, the -OH groups are protonated and can adsorb F^- through exchange mechanism. At acidic pH, the fluoride adsorption capacity is diminished probably due to formation of HF and at alkaline pH value, fluoride

adsorption is also lower due to competition with -OH ions. Patnaik *et al*. (2016) reported chitosan-Fe^{3+} complex, Sundaram *et al*. (2009) studied magnesia/chitosan composite, Swain *et al*. (2009) investigated aluminium impregnated chitosan biopolymer and Jagtap *et al*. (2011) reported lanthanum impregnated chitosan flakes for fluoride removal as presented in table 4.

Table 4: Summary of electropositive multivalent metal incorporation method of biopolymer adsorbents

Adsorbent Material	**Q_{max} (mg/g)**	**Optimal pH**	**Isotherm Model**	**Kinetic Model**	**Thermody-namics**	**Mechanism Proposed**	**Adsorbent Characterization**	**Reference**
Chitosan-Fe^{3+} complex	2.34	3.0-10.0	Langmuir-Freundlich and D-R isotherm	Pseudo-second-order	Spontaneous and exothermic	Ion exchange	FTIR and SEM	Patnaik *et al*., 2016
Magnesia / Chitosan Composite	11.24	10.6	Langmuir and Freundlich	Pseudo-second-order, particle and intraparticle diffusion	Spontaneous and Endothermic	Electrostatic attraction, hydrogen bonding	FTIR and SEM with EDAX	Sundaram *et al*., 2009
Aluminium impregnated chitosan biopolymer	-	6.5	Freundlich	Pseudo first-order	spontaneous and endothermic	chemical surface precipitation/ligand exchange	FTIR and SEM-EDS	Swain *et al*., 2009
Lanthanum impregnated chitosan flakes	1.27	6.7	Freundlich	Pseudo second order and intraparticle diffusion	-	Electrostatic attraction	FTIR, SEM and XRD	Jagtap *et al*., 2011

4.4 Quaternization of $-NH_2$ to $-N^+(CH_3)_3$: The quaternization of chitosan (CS), involving the addition of methyl or larger alkyl groups with or without spacers, or modifying CS before quaternization, introduces a permanent positive charge (Žigrayová *et al*., 2024). This modification enhances the solubility across a wide pH range and often improves the antimicrobial properties, biocompatibility and biodegradability.

The amino ($-NH_2$) in chitosan reacts more rapidly and effectively, providing better protection for other functional groups. This is because the C2-NH_2 group has a strong nucleophilic lone pair of electrons (Zigrayova *et al*., 2024). Depending on the reaction conditions such as pH, C3–OH^- and C6-OH^- protection groups may be recommended (Benediktsdóttir *et al*., 2014). Quaternization of chitosan with methyl iodide yields N.N.N-trimethyl chitosan with a quaternary ammonium group ($^+$NR4) bearing a permanent positive charge and an iodide (I^-) as the counter ion as presented in figure 1.

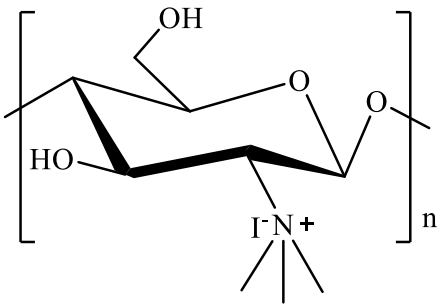

Figure 1: Quaternary ammonium chitosan (Zigrayova *et al*., 2024)

The simplest method for the synthesis of N,N,N-trimethyl chitosan (TMC) is a one-step reaction where CS is treated with methyl iodide (CH_3I) under strongly alkaline conditions, using N-methyl-2-pyrrolidone (NMP) as the solvent and sodium iodide (NaI) as the catalyst. This process typically results in a quaternization degree ranging from 10-45%.Quaternization may also be achieved using dimethyl sulphite (DeBritto and Assis, 2007). According to Benediktsdôttir *et al*. (2011), O-methylation of the $-OH^-$ groups can yield a homopolymer TMC. Tert-butyldimethylsilyl (TBDMS) protected polymer has good solubility in a wide variety of organic solvents, such as NMP enabling modification of amino groups on the polymer backbone (Benediktsdôttir *et al*., (2011).

The F^- is mainly removed from the bulk solution by displacing I^- from the quaternary ammonium (Mawira *et al*., 2023). The ion exchange is favored due to F- having smaller size, higher charge density, higher polarizing power and hydration energy compared to I^- with larger size, lower charge density, more polarizable and lower hydration energy. The F^- is electrostatically attracted to the permanent change on $^+NR_4$ (Mwangi *et al*., 2019) increasing local concentration near the adsorbent hence facilitating the ion exchange mechanism. Table 5 summarizes the activation methods involving chitosan biopolymer adsorbents.

Table 5: Summary of quaternization method of biopolymer adsorbents

Adsorbent Material	**Q_{max} (mg/g)**	**Optimal pH**	**Isotherm Model**	**Kinetic Model**	**Thermody-namics**	**Mechanism Proposed**	**Adsorbent Characterization**	**Reference**
Quaternized aminated cellulose	3.6311	4	Langmuir	-	-	Adsorption and ion exchange	FTIR and TGA	Mawira *et al*., 2023

5. Crosslinking Methodologies

Cross-linking with a suitable cross-linking agent produces chemical bonds between biopolymer chains and generates a strong three-dimensional network. Depending on the existing active groups and compatibility, the cross-linking agent may cause covalent, ionic or physical cross-linking (Yammine *et al*., 2025). The nature of bonding determines the properties and applications of the cross-linked material.

Chitosan with molecular weight lower than 1×10^4 g/mol can be cross-linked to enhance mechanical, structural and thermal properties (Mandera-Santana *et al*., 2018; Valdez-Alegria *et al*., 2020). Cross-linking also inhibits swelling and prevents them from dissolving in surrounding aqueous media (Shaumbwa *et al*., 2021). According to Tillet *et al*. (2011), cross-linking of chitosan can be performed at room temperature or above room temperature. The cross linking agents used at room temperature are those capable of reacting with the amine group of chitosan in aqueous solution. Typically, enzymatic reactions and the physical cross-linking of chitosan are performed at room temperature. The main uses

of this type of cross-linking agents are in coatings, hydrogels, blend films of protein-polysaccharide among others.

The use of a specific temperature (between 40 and 150°C) is required because the chemical reaction involving different functional groups occurs easily, some cross-linking agents exhibiting double reactivity and self-cross-linking among other characteristics.

5.1 Types of Crosslinking

5.1.1 Chemical (Covalent) Crosslinking: This involves formation of new covalent bonds between polymer chains (or within a chain) to form stable biopolymer networks.

This is used to enhance stiffness and strength (Žigrayová *et al*., 2024) in hydrogels and adsorbents where strong bonds are required to resist significant stress (Yammine *et al*., 2025). The method is very versatile: crosslinkers can target different functional groups (–OH, –NH_2, –COOH). Examples: epoxide-based crosslinkers (e.g., epichlorohydrin, diglycidyl ethers e.t.c), aldehydes (glutaraldehyde, formaldehyde e.t.c), carboxylic acids (citric acid) and natural crosslinkers like genipin.

5.1.2 Physical Crosslinking: This polymer network occurs through combination of ionic, hydrophobic, and hydrogen-bonding interactions, influenced by factors such as temperature, pH and ionic strength. Their mechanical strength is lower compared to covalent networks. However, it is advantageous due to reduced toxicity and the ability to control properties like swelling and degradation.

5.1.2.1 Ionic Crosslinking: This is based on electrostatic interactions between oppositely charged groups on polymer chains. These bonds are often reversible, dynamic and less rigid compared to covalent networks, making these materials more flexible and responsive to environmental changes such as pH (Yammine *et al*., 2025). Examples: alginate by calcium ions to form a hydrogel (Yammine *et al*., 2025). In acidic media, polycationic chitosan interacts electrostatically with negatively charged triphosphate (TPP) to form intermolecular and intramolecular network as shown in figure 2.

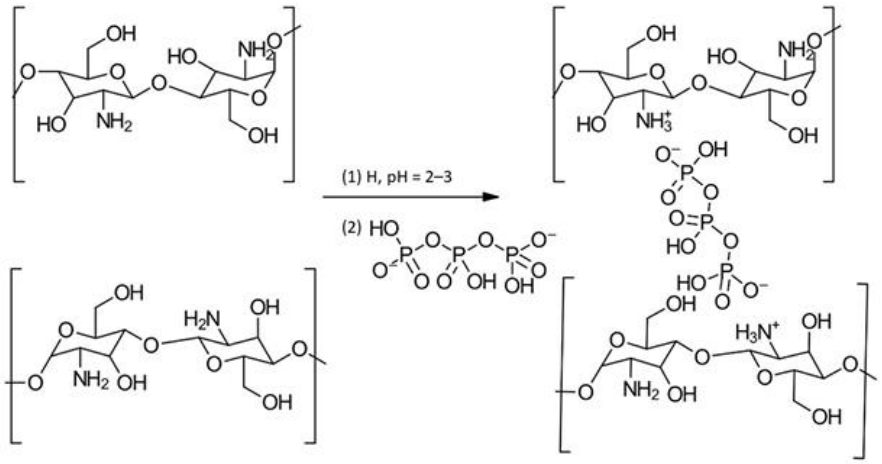

Figure 2: Scheme of chitosan-TPP crosslinking (Žigrayová *et al*., 2024)

5.1.2.2 Hydrogen Crosslinking: This is observed due to interactions between hydrogen atoms and electronegative atoms such as oxygen or nitrogen (Yammine *et al*., 2025). These types of bonds are weaker than covalent and ionic bonds. It enhances elasticity and self-healing properties particularly in biopolymers. In poly vinyl alcohol (PVA), hydrogen crosslinking involves hydrogen bond formation between hydroxyl groups on the polymer chains or other chemical species (Yammine *et al*., 2025). Other hydrogen-bonding crosslinkers include polyethylene glycol (PEG), carboxymethyl cellulose (CMC), dextrin and chitosan. The type of crosslinking chosen depends on the desired properties such as flexibility, strength, responsiveness and versatility.

Likewise diverse crosslinkers exist such as glutaraldehyde, epichlorohydrin and poly (ethylene glycol) diglycidyl ether (PEGDE) and their choice depends on a number of factors such as the desired properties, application and crosslinking mechanism and chemistry. Crosslinking success is confirmed using different characterization techniques such as FTIR (Vijaya *et al*., 2011; Barbosa *et al*., 2025), SEM (Valdez-Alegria *et al*., 2020), solid state ^{13}C NMR, swelling tests (Chang *et al*., 2009; Barbosa *et al*., 2025), change in mechanical strength (Chang *et al*., 2009) and thermal stability (Bashandeh & Khalaji, 2021).

5.2 Mechanism of Crosslinking by Different Crosslinkers

5.2.1Epichlorohydrin (ECH): ECH is a small epoxy molecule (1-chloro-2,3-epoxypropane) that contains an epoxide ring and a chloromethyl group. Crosslinking with ECH often happens under alkaline conditions (e.g., NaOH) to promote ring opening of the epoxide. In basic media, nucleophiles (e.g., –OH or $–NH_2$ on the biopolymer) attack the epoxide ring of ECH (Yammine *et al*., 2025). For chitosan, the hydroxyl (–OH) groups are primary nucleophiles. The epoxide ring opens, forming an ether linkage (–C–O–C) between ECH and the biopolymer chain. The chloromethyl side of ECH can also react (or be displaced), potentially leading to further crosslinking or branching. Chitosan has amino ($–NH_2$) and hydroxyl (–OH) functional groups. ECH can react with both, but under typical conditions (alkaline) it preferentially crosslinks through the hydroxyl groups of chitosan, rather than the amines as shown in figure 3.

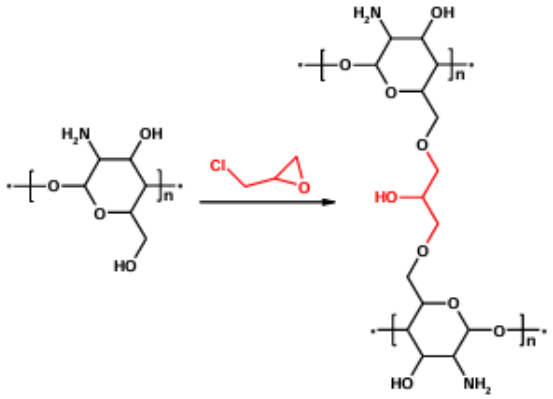

Figure 3: Scheme of chitosan-epichlorohydrin crosslinking (Bashandeh & Khalaji, 2021)

The reaction temperature is maintained at 45˚C to accelerate the reaction (Jawad *et al*., 2019). Some studies indicate ECH can also link via amine, but the dominant reaction under typical base catalysis is with –OH. According to Dong *et al*. (2017), protection of the reactive $–NH_2$ groups and subsequent deprotection may still be required to homogenously form linkages at the C6–OH^- groups and preserve a higher number of $–NH_2$ active sites.

Yan & Yuan (2001) reported successful benzaldehyde protection and HCl solution deprotection of C2-NH_2 in chitosan following characterization. Cross-linking with ECH improves mechanical stability, chemical resistance, reusability, and often adsorption performance (for adsorbent uses) by stabilizing the chitosan matrix. For example, crosslinked chitosan beads show higher adsorption capacity and reusability.

5.2.2 Glutaraldehyde: A classical crosslinker for chitosan, reacting primarily via Schiff base (imine bond) formation between the aldehyde groups of glutaraldehyde and the amino ($–NH_2$) groups of chitosan (Barbosa *et al*., 2025: Yammine *et al*., 2025). It is highly reactive and gives strong covalent networks, but disadvantages include reduction in the number of free amino groups which may be critical for adsorption (Barbosa *et al*., 2025). Crosslinking in chitosan begins with nucleophilic attack by the amino group's free electrons on the electrophilic carbonyl carbon of the glutaraldehyde's aldehyde group forming a hemiketal intermediate, which is unstable (Yammine *et al*., 2025).The hemiketal

intermediate undergoes dehydration (loss of water) followed by deprotonation to form a stable imine (Schiff base) linkage (Barbosa *et al.*, 2025). This reaction involves the formation of a double bond between the nitrogen of the amino group and the carbon of the carbonyl group, resulting in the loss of water.

The imine group formed in the previous step can further react with another aldehyde group from a second glutaraldehyde molecule or from another lysine residue, leading to the formation of a covalent crosslink between two molecules. This creates a three-dimensional network of crosslinked molecules as shown is figure 4.

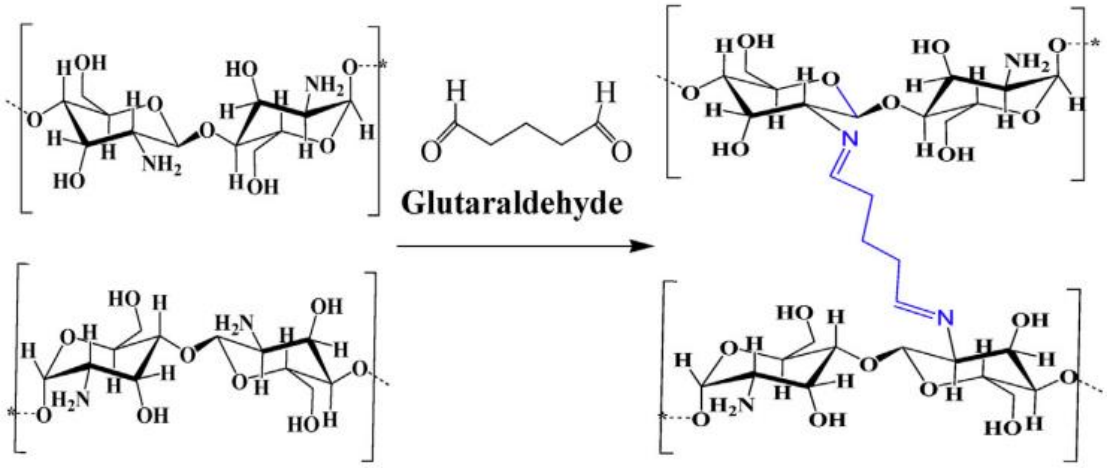

Figure 4: Scheme of chitosan-glutaraldehyde crosslinking (Isam *et al.*, 2019)

5.2.3 Diglycidyl Ethers / Multi-epoxy Agents: Examples include ethylene glycol diglycidyl ether (EGDE) and multi-epoxy crosslinkers. These crosslink via epoxide opening similar to ECH. They allow tuning of crosslink density, network architecture (e.g., branching) depending on the number of epoxide groups. The resulting network is presented in figure 5.

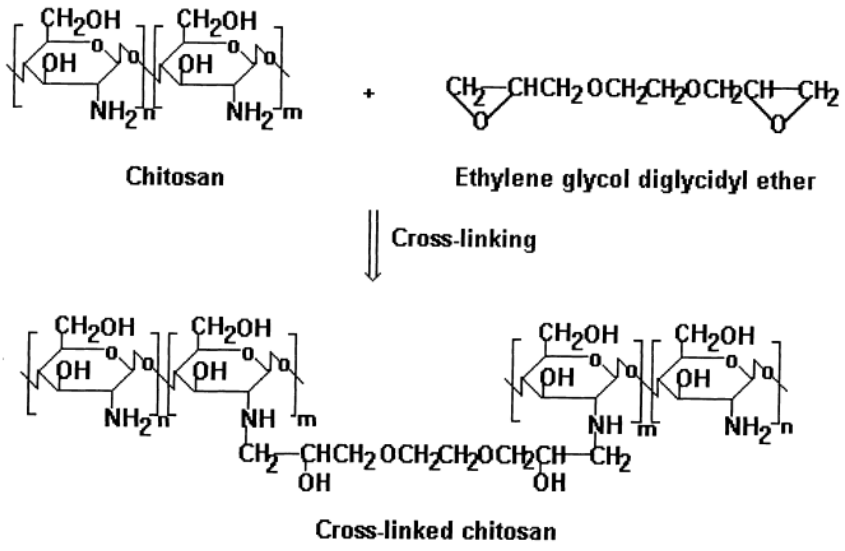

Figure 5: Scheme of chitosan-ethylene glycol diglycidyl ether crosslinking (Zeng & Ruckenstein, 1998)

5.2.4 Genipin: A natural crosslinker, lower toxicity, often used in biomedical hydrogels. It reacts with primary amines as shown in figure 6.

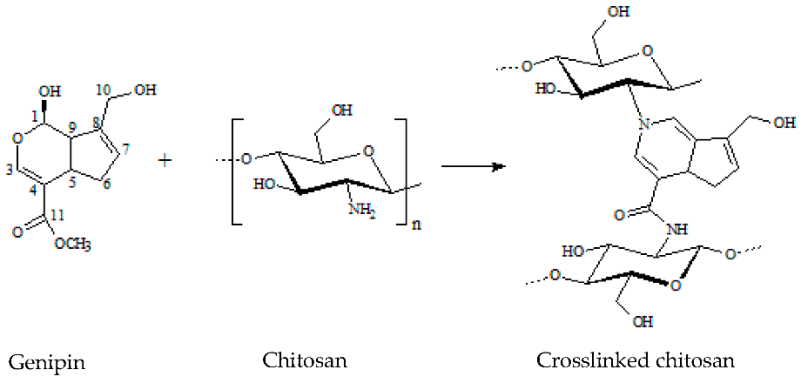

Figure 6: Scheme of chitosan-genipin Crosslinking (Pomari *et al.*, 2019)

5.2.5 Carboxylic Acids (e.g., Citric Acid): Citric acid can crosslink via esterification (–COOH with –OH), under appropriate conditions. Citric acid, a natural metabolite, is a non-toxic, renewable and bio-based reagent which could react with the chitosan amines to form an amide structure as shown in figure 7.

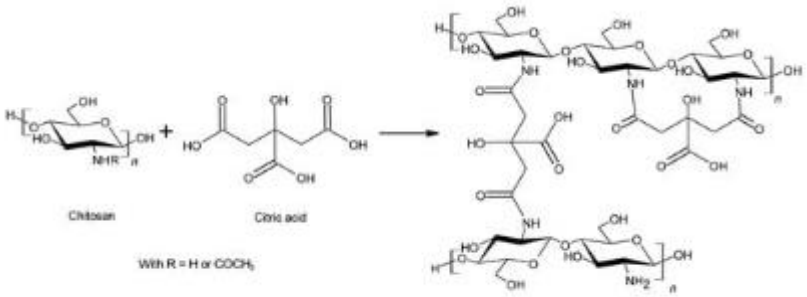

Figure 7: Scheme of chitosan-citric acid crosslinking (Silvestre *et al.*, 2021)

Table 6 summarizes different cross-linking agents used for biopolymers, characterization, application, adsorption capacity, isotherm and kinetic models.

Table 6: Summary of biopolymer material, crosslinker, characterization, application, adsorption capacity, isotherm and kinetic models.

Material	Crosslinker	Characterization	Application	Adsorption capacity	Isotherm	Kinetics	Reference
Chitosan	Glutaraldehyde	FTIR, SEM, Swelling test and sorption assays	Removal of heavy metals (copper and chromium)	Cu-0.422 $mmolg^{-1}$ Cr-1.143 $mmolg^{-1}$	Langmuir	Pseudo second order	Barbosa *et al.*, 2025
Chitosan-Polyvinyl alcohol hydrogel	Sodium tripolyphosphate pentabasic (TPP)	FTIR, SEM, %Moisture, PZC and BET	Fluoride Removal	12.64 mgg^{-1}	Freundlich	Pseudo second order	Valdez-Alegria *et al.*, 2020
Pectin-alginate based biomaterial scaffolds	Glutaraldehyde and trimetallic oxide Fe-Al-Ce	XPS	Fluoride Removal	400 mgg^{-1}	Langmuir	Pseudo second order	Raghav *et al.*, 2019

La^{3+} impregnated crosslinked gelatin	Glutaraldehyde	-	Fluoride Removal	98.8%	-	Pseudo first order	Zhou *et al.*, 2004
Cross-linked chitosan	Epichlorohydrin	FTIR, XRD, TGA-DTA and DSC	Methyl Green Removal	92.7%	-	-	Bashandeh and Khalaji , 2021
Chitosan and gelatin	Glutaraldehyde	FTIR, FE-SEM, XPS and swelling tests	Heavy metals: Pb (II), Cd (II), Hg (II) and Cr (III)	98% for Hg (II)	-	-	Perumal *et al.*, 2019
Chitosan and Fe	Ethylene glycol diglycidyl ether	FTIR, XPS, BET, PZC	Fluoride removal	295 mgg^{-1}	Langmuir-Freundlich	Pseudo first order	Arcos-Arévalo *et al.*, 2016

6. Characterization of Biopolymer Nanocomposites

Biopolymer nanoparticles have different structural and physical properties such as composition, concentration, size, shape, surface properties, crystallinity and crosslinking mechanisms (Bergstrom, 2015). In recent years, characterization techniques have emerged to help researchers understand structural characteristics of nanomaterials better.

6.1 Surface Morphology: The properties and performance of the nanoparticles depends on the size, shape, surface structure and interparticle interaction which are investigated using one or combination of the following techniques:

6.1.1 Scanning Electron Microscopy-Energy Dispersive X-Ray Spectroscopy (SEM-EDS): SEM with EDS is used to determine the surface morphology and elemental composition of the sample (Mutalib, *et al*., 2017). SEM can give information about the sample including texture, chemical composition, crystalline arrangement (Perumal *et al*., 2019), and orientation of constituents making up the sample. In addition to these, SEM can identify and analyze surface fractures, inspect surface contaminations, reveal spatial variations in chemical compositions, and identify crystalline structures (Mayeen *et al*., 2018).

In SEM, a focused beam of electrons react with the sample to produce secondary electrons (SEs), backscattered electrons, and characteristic X-ray, which is then detected with respective detectors and finally displayed on the monitor.

EDX analysis focuses on the characteristic X-ray generated by SEM. The X-rays emitted from the specimen give information as to the elemental composition of the area. Thus, the EDS technique can detect elements from carbon to uranium in extremely low quantities ranging to 1.0 wt % (Mayeen *et al*., 2018).

6.1.2 Transmission Electron Microscopy (TEM): TEM enables high magnification imaging to examine specimen microstructure, crystallinity, lattice distortion, chemical composition and morphology as reported previously Kotrbova *et al*. (2019). In TEM analysis, an incident electron beam penetrates the sample and separates into transmitted and diffracted components both carrying structural information. These beams are refracted by the objective lens and brought to distinct focal positions where ordered spot patterns corresponding to the crystal diffraction are formed.

As the beams propagate beyond the objective focal plane, they gradually converge and overlap at the image plane producing a real space image that is recorded by a CCD detector through subsequent electromagnetic lenses. Owing to its extremely high spatial resolution, this technique allows detailed observation of defects from both planar and cross sectional views enabling atomic scale defect identification (Cui *et al*., 2023).

6.1.3 Atomic Force Microscopy (AFM): AFM generates surface images by monitoring the interaction forces between a sharp probe and the sample which serve as the feedback signal. During measurement, a nanoscale tip attached to a flexible cantilever is raster scanned across the sample surface. A control system continuously regulates the tip–sample interaction by adjusting the vertical position of the scanner to maintain a constant force. The recorded height adjustments as a function of lateral position are then converted into a topographical map of the surface as described in earlier studies (Mayeen *et al*., 2018).

6.1.4 Scanning Tunneling Microscopy (STM): The STM technique is based on quantum tunneling current to create electron density images for conductive or semiconductive surfaces and biomolecules attached on conductive substrates at the atomic scale.

A probe is brought in close vicinity to the surface of an object measured to monitor the reactions of the probe. As per the tip-sample, separation is maintained in the range of 4–7 A˚, a small voltage given amid the scanning tip and the surface reasons tunneling of electrons by which variation of the resulting current can be recorded while the tip moves across the sample in the x–y plane to generate a map of charge density (Mayeen *et al*., 2018; Yang & Freund, 2024). Recent articles highlight advancements in HS-STM systems that can capture images at video rates (up to 100 frames per second or more), enabling the study of dynamic surface processes in real-time, such as atom diffusion, on-surface synthesis, and chemical reactions (Yang & Freund, 2024) Furthermore, researchers have introduced a machine learning approach to automatically identify the atomic structure and chemical species directly from experimental bond-resolved STM images (Kurki *et al*., 2024).

6.2 Chemical Composition and Crystal Structure: Chemical composition refers to atomic elements within the nanoparticles and the formed functional groups while crystal structure is the organization of elemental atoms in a nanoparticle into a crystal structure or it may be amorphous (Zielinska *et al*., 2020).

6.2.1 Fourier Transform Infrared Spectroscopy (FTIR): The FTIR technique is used to determine the functional groups in the adsorbent using infrared radiation (Mwangi *et al*., 2019; Ndiritu *et al*., 2020; Tazik *et al*., 2023). When infrared radiation illuminates a sample, the bonds in IR active molecules absorb light creating vibration modes such as twisting, wagging, scissoring and rocking (Khan *et al*., 2018).

6.2.2 Atomic Absorption Spectroscopy (AAS): Atoms in unexcited state are generated at the atomizing component and jump to excited state upon absorption of appropriate radiation at specific wavelength. The sample absorbance is proportional to concentration of metallic pollutant computed from the standard calibration curves (Siraj & Kitte, 2023).

6.2.3 X-Ray Diffraction (XRD): XRD is widely applied to investigate material microstructural characteristics such as lattice spacing, crystalline order, preferred orientation and the presence of structural defects (Bashandeh & Khalaji, 2021). In a typical analysis, the polymer specimen is irradiated with monochromatic X rays of short wavelength approximately 0.1 nm. As the beam penetrates the sample, its intensity decreases exponentially according to I equals I_0 exp(-μx), where I_0 is the initial intensity and μ represents the linear absorption coefficient, indicating that penetration depth is governed by both material properties and X ray energy.

During interaction with the specimen, a fraction of the incident radiation is absorbed while another portion is scattered or transmitted without change. Scattering arises from interactions between X rays and the electron clouds of atoms within the material. Constructive interference among the scattered waves produces diffraction peaks whose positions and intensities are determined by the incident angle and crystallographic arrangement of the sample (Bergstrom 2015).

6.2.4 X-Ray Photoelectron Spectroscopy (XPS): XPS the sample surface is irradiated with X rays causing electrons to be emitted from core and valence energy levels of surface atoms. These emitted photoelectrons are collected and analyzed using a hemispherical energy analyzer that determines their kinetic energy. From the measured kinetic energy, the corresponding binding energy relative to the Fermi level is calculated. Shifts in binding energy commonly referred to as chemical shifts arise when the oxidation state or local electronic environment of an element changes as a result of different chemical bonding or coordination conditions (Krishna & Philip, 2022).

6.3 Thermostability

Thermogravimetric analysis is used to determine polymer degradation temperatures (Bashandeh & Khalaji, 2021), residual solvent levels, absorbed moisture content and the amount of inorganic (noncombustible) filler in polymer or composite material compositions (Bergstrom 2015).

6.3.1 Thermogravimetric Analysis (TGA): The technique is used to study weight change of a sample as a function of time or temperature (Loganathan *et al*., 2017; Mwangi *et al*., 2019). It is useful in studying thermal events such as absorption, adsorption and desorption among others. TGA can also be utilized for evaluation of volatile or gaseous products lost during such chemical reactions for samples such as nanomaterials and polymers among others (Mwangi *et al*., 2019).

6.4 Surface Area and Chemistry

For nanoparticles, a higher proportion of atoms are on their surfaces, (due to higher area/volume ratio) and these atoms are in direct contact with solvents and influence their interactions with other molecules (Bergstrom 2015).

6.4.1 N_2 Adsorption-Desorption Study: The surface area of nanoporous gold materials is typically expressed as the BET specific surface area SBET derived from nitrogen adsorption–desorption measurements conducted at 77 K using the Brunauer Emmett and Teller approach. Gas physisorption techniques employing inert probe molecules such as nitrogen argon or krypton are widely used to evaluate the surface characteristics and pore structure of porous solids. Owing to the availability of automated commercial analyzers with integrated data processing, nitrogen adsorption experiments at cryogenic temperature have become a routine method for characterizing newly developed materials. These systems quantify the amount of adsorbed nitrogen through gravimetric volumetric or continuous flow measurement modes. Surface area values are obtained by fitting the experimental adsorption isotherm with an appropriate theoretical model most commonly the BET equation which assumes distinct adsorption energies for the first molecular layer and for subsequent multilayer formation corresponding respectively to the heat of adsorption and the heat of liquefaction (Tan *et al*., 2012).

6.5 Zeta Potential

It is a measure of the difference between a nanoparticle's electrostatic potential and that of the bulk solution. To obtain the zeta potential, a laser is passed through a nanoparticle solution under the influence of a varied electric field (Bergstrom, 2015).

6.5.1 Laser Doppler Electrophoresis: An electric potential is applied across electrodes at opposite ends of a cell containing a particle suspension, causing charged particles to migrate toward the electrode of opposite polarity. The velocity of these particles under the applied field is used to calculate their

electrophoretic mobility. In laser Doppler electrophoresis, the motion of the particles induces small shifts in the frequency of scattered light. The frequency shift Δf is given by,

$$\Delta f = \frac{2v\sin(\frac{\theta}{2})}{\lambda} \quad (4)$$

where v is the particle velocity, λ is the laser wavelength and θ is the scattering angle. The measured electrophoretic mobility U_E is converted into zeta potential (ξ) using Henry's equation (5).

$$U_E = \frac{2\varepsilon\xi F(Ka)}{3\eta} \quad (5)$$

where ε is the dielectric constant of the medium, η is the viscosity and F(ka) is the Henry function (Kaszuba *et al*., 2010). This method allows precise determination of the surface charge characteristics of dispersed particles.

6.6 Molar Mass Distribution

This can provide information regarding the influence of formulation components on the polymerization process and degradation of the polymer (Zielinska *et al*., 2020).

6.6.1 Size Exclusion Chromatography (SEC): In SEC, a solvent is forced through the column at rates typically 1 ml/min and pressures of 50-200 bar. The column diameter is 10 mm and length of 500-1000 mm, packed with a porous material (typically silica or crosslinked polystyrene).

A sample is dissolved in the same solvent that is running through the column and is then introduced into the solvent stream going through the column. A detector monitors the concentration of sample exiting the end of the column. Inside the column, molecules are separated based on their hydrodynamic volume. For polymers this can vary greatly with the particular solvent and the temperature. By studying the properties of polymers in particular solvents and by calibrating each column setup with samples of known molecular weight, it is possible to get a relative distribution of molecular weights for a given polymer sample. Using this data, it is possible to calculate number-average molecular weight, weight-average molecular weight, polydispersity, as well as higher order molecular weights within a high level of accuracy (Bergstrom 2015).

6.7 Crosslinking Success

6.7.1 Fourier-Transform Infrared Spectroscopy (FTIR / ATR-FTIR): The spectra of native vs crosslinked chitosan are compared to investigate reduction in -OH band intensity (broad –OH stretch), shifts in band of C-N (Barbosa *et al*., 2025), changes in N–H or C–N modes, appearance of new ether link (C–O–C) signals, or other bonds (Vijaya *et al*., 2011). For example, in ECH-crosslinked chitosan beads, FTIR has been used to confirm the reaction between ECH and the primary hydroxyl group. Vijaya *et al*. (2011) confirmed fluoride adsorption using glutaraldehyde crosslinked calcium alginate due to appearance of a new band at 745 cm^{-1}. Barbosa *et al*. (2025) observed the change in the 1636 cm^{-1} region with the presence of a single peak, which could be associated with the imine group (C=N), indicating the success of cross-linking of the hydrogel. The shift for the band of C-N to 1406 cm^{-1} signified interaction in the region while appearance of bands at 1554 and 1383 cm^{-1} was associated with C-H stretching, related to the glutaraldehyde chain.

6.7.2 Swelling Tests / Gel Fraction: The degree of swelling in a solvent (e.g., water, buffer) is measured. A strongly crosslinked network will swell less (Chang *et al*., 2009).

According to Barbosa *et al*. (2025) extreme crosslinking promotes a reduction of available groups able to absorb water and may also impact the potential removal of contaminants.

6.7.3 Mechanical / Rheological Testing: The biopolymer sample is subjected to mechanical analysis to evaluate changes in mechanical strength (Chang *et al*., 2009). Rheometry (dynamic mechanical analysis): measure storage (G′) and loss (G″) moduli; crosslinked networks often show gel-like behavior (G′ > G″) and characteristic gel points.

6.7.4 Thermal Analysis

- **Differential Scanning Calorimetry (DSC):** crosslinked materials may show changes in glass transition temperature (Tg), melting transitions, or thermal events due to a more rigid network (Tandon *et al*., 2017; Bashandeh & Khalaji, 2021).
- **Thermogravimetric Analysis (TGA):** crosslinked biopolymers often show enhanced thermal stability (shift in degradation onset) because the network restricts chain mobility (Zhang *et al*., 2017).

6.7.5 Morphological / Structural Imaging: Scanning Electron Microscopy (SEM): examine surface morphology, porosity, microstructure; crosslinking often changes surface roughness, porosity (Perumal *et al*., 2019). Example: crosslinked chitosan adsorbents showed increased roughness. Barbosa *et al*. (2025) observed a highly porous chitosan-glutaraldehyde hydrogel structure with a pore size of 23.6 ± 6.8 µm. **X-ray Diffraction (XRD)**: Used to see changes in crystallinity (crosslinking may reduce or rearrange crystalline domains) (Bashandeh & Khalaji, 2021).

6.7.6 Site-Specific / Molecular-Level Probing

Nuclear Magnetic Resonance (NMR): Solid-state ^{13}C NMR has been reported as a useful characterization technique for insoluble crosslinked networks since it can reveal new carbon–oxygen linkages (ether carbons) and changes in chemical shifts of carbons near crosslinked sites (Benediktsdóttir *et al*., 2014). Solution NMR (if possible): if fragments or soluble parts exist, one can examine the chemical environment of –OH / $–NH_2$ carbons.

6.7.7 Point of Zero Charge (PZC): Crosslinking often modifies functional groups (e.g., consumes $–NH_2$, –OH, –COOH) on the biopolymer chains, or changes their accessibility and the functional groups that contribute to surface charge (via protonation/deprotonation) may become less available leading to shifts in PZC value (Arcos-Arévalo *et al*., 2016; Valdez-Alegria *et al*., 2020).This test is used to complement other crosslinking characterization techniques such as FTIR.

6.7.8 Percentage Moisture Analysis: Crosslinking restrict how much the polymer chains can move. More crosslinking means a denser polymer network and less free volume for water to penetrate or occupy. As crosslink density increases, the mesh size (distance between crosslinks) typically shrinks. That means less space for water, so equilibrium water content goes down (Valdez-Alegria *et al*., 2020). This test complements other crosslinking characterization techniques such as FTIR.

7. Conclusions and Future Perspectives

A substantial number of articles on emerging aspects on biopolymer adsorbents and important insights were consolidated. The analysis found that current research is focused on development and modification of efficient, selective, low cost and safe adsorbents for fluoride removal from drinking water. Most of the fabricated adsorbents especially metal doped adsorbents concentrated on enhancing adsorption capacity but failed to address setbacks associated with the conventional adsorbents such as safety to human and environment, cost of raw materials, recovery challenges and competitive adsorption in actual water.

Crosslinking modification with the appropriate crosslinker was widely reported to increase porosity and adsorption capacity of biopolymer composites. The emerging nanoscale technology is a

game changer in biopolymer modification with biopolymer nanocomposites exhibiting enhanced adsorption performance.

This thorough review found crosslinked biopolymers nanocomposites such as chitosan nanocomposites and chitosan blended nanocomposites as promising adsorbents that if well synthesized could solve the limitation with most conventional adsorbents.

Future research should focus on applying safe activation methods and enhancing porosity, safety, efficiency, stability, mechanical strength and selectivity in biopolymer nanocomposite fabrication.

Funding: The research did not receive funding.

Conflicts of Interest/Competing Interests: The authors declare no competing interests.

Ethics Approval: Not applicable.

Data and/or Code Availability: Not applicable.

Authors' Contribution: Paul M. Munene wrote and reviewed the manuscript while Nthiga E.W reviewed the manuscript.

References

[1]. Abanyie, S., Ampadu, B., Frimpong, N., & Amuah, E. (2023). Impact of improved water supply on livelihood and health: Emphasis on Doba and Nayagnia, Ghana. *Innovation and Green Development, 2*(1), 1-9. https://doi.org/10.1016/j.igd.2023.100033

[2]. Aboulsoud, Y. I. E. (2024). Biosorptive removal of fluoride from wastewater using tea domestic waste biochar. *Environment, Development and Sustainability*, *27*(7), 16451–16468. https://doi.org/10.1007/s10668-024-04598-2

[3]. Akafu, T., Chimdi, A., & Gomoro, K. (2019). Removal of fluoride from drinking water by sorption using diatomite modified with aluminium hydroxide. *Journal of Analytical Methods in Chemistry*, *2019*, 1–11. https://doi.org/10.1155/2019/4831926

[4]. Alkurdi, S. S. A., Al-Juboori, R. A., Bundschuh, J., & Hamawand, I. (2019). Bone char as a green sorbent for removing health threatening fluoride from drinking water. *Environment International*, *127*, 704–719. https://doi.org/10.1016/j.envint.2019.03.065

[5]. Araga, R., Soni, S., & Sharma, C. S. (2017). Fluoride adsorption from aqueous solution using activated carbon obtained from KOH-treated jamun (*Syzygium cumini*) seed. *Journal of Environmental Chemical Engineering*, *5*(6), 5608–5616. https://doi.org/10.1016/j.jece.2017.10.023

[6]. Arcibar-Orozco, J. A., Flores-Rojas, A. I., Rangel-Mendez, J. R., & Díaz-Flores, P. E. (2020). Synergistic effect of zeolite/chitosan in the removal of fluoride from aqueous solution. *Environmental Technology*, *41*(12), 1554–1567. https://doi.org/10.1080/09593330.2018.1542033

[7]. Arcos-Arévalo, A., Zavula-Arce, R., Ávila-Pérez, P., García-Gaitán, B., García-Rivas, J., & Jiménez-Núñez, M. (2016). Removal of fluoride from aqueous solutions using

chitosan cryogels. *Journal of chemistry*, *2016*, 1-13. http://dx.doi.org/10.1155/2016/7296858

[8]. Barbosa, R.F., Shyam, S., Misra, S., Mitra, S.K., & Rosa, D.S. (2025). Chitosan hydrogels crosslinked with glutaraldehyde for potential toxic elements removal: Batch and purification analysis. *Journal of Applied Polymer Science*, *142*(39), 1-15. https://doi.org/10.1002/app.57539

[9]. Bashandeh, Z., & Khalaji, A.D. (2021). Effective removal of methyl green from aqueous solution using epichlorohydrine cross-linked chitosan. *Advanced Journal of Chemistry-Section A*, *4*(4), 270-277. https://doi.org/10.22034/ajca.2021.285520.1259

[10]. Benediktsdôttir, B.E., Gaware, V.S., Růnarsson,Ö.V., Jônsdôttir, S., Jensen, K.J., & Mâsson, M. (2011). Synthesis of N,N,N-trimethyl chitosan homopolymer and highly substituted N-alkyl, N,N-dimethyl chitosan derivatives with the aid of di-tert-butyldimethylsilyl chitosan. *Carbohydrate Polymers*, *86* (4), 1451-1460. https://doi.org/10.1016/j.carbpol.2011.06.007

[11]. Benediktsdóttir, B.E., Baldurson, Ó., & Masson, M. (2014). Challenges in evaluation of chitosan and trimethylated chitosan (TMC) as mucosal permeation enhancers: From synthesis to *in vitro* application. *Journal of Controlled Release*, *173*, 18-31. https://doi.org/10.1016/j.jconrel.2013.10.022

[12]. Bergström, J. S. (2015). Experimental characterization techniques. In *Mechanics of solid polymers: Theory and computational modeling* (pp. 19–114). William Andrew.

[13]. Cai, J., Zhao, X., Zhang, Y., Zhang, Q., & Pan, B. (2018). Enhanced fluoride removal by La-doped Li/Al layered double hydroxides. *Journal of Colloid and Interface Science*, *509*,353–359. https://doi.org/10.1016/j.jcis.2017.09.038

[14]. Chang, C., Duan, B., & Zhang, L. (2009). Fabrication and characterization of novel macroporous cellulose-alginate hydrogels. *Polymer*, *50*, 5467-5473. https://doi.org/10.1016/j.polymer.2009.06.001

[15]. Chang, G., Li, W., Cao, J., Wang, Z., Tan, X., & Wang, X. (2024). Aluminium alginate foam synthesis, characterization and application for low concentration fluoride ion removal. *Desalination and Water Treatment*, *317*, 100156. https://doi.org/10.1016/j.dwt.2024.100156

[16]. Cui, Y., Wang, C., Liu, X., Wu, Y., Li, Z., Li, R., &He, W. (2023). A review of subsurface damage detection methods for optical instruments. *American Institute of Physics Advances*, *13*, 60702-60709. https://doi.org/10.1063/5.0151498

[17]. De Britto, D., & Assis, O.B. (2007). A novel method for obtaining a quaternary salt of chitosan. *Carbohydrate Polymers*, *69*(2), 305–310. https://doi.org/10.1016/j.carbpol.2006.10.007

[18]. Devi, R.R., Umlong, I.M., Raul, P.K., Das, B., Banerjee, S., & Singh, L. (2014). Defluoridation of water using nano-magnesium oxide. *Journal of Experimental Nanoscience*, *9*(5), 512-524. https://doi.org/10.1080/17458080.2012.675522

[19]. Dhawane, S. H., Khan, A. A., Singh, K., Tripathi, A., Hasda, R., & Halder, G. (2018). Insight into Optimization, Isotherm, Kinetics, and Thermodynamics of Fluoride Adsorption onto Activated Alumina. *Environmental Progress and Sustainable Energy*, *37* (2), 766–776. https://doi.org/10.1002/ep.12814

[20]. Dong, L., Wen, C., & Yigang, D. (2017). Synthesis of carboxyl-introduced chitosan with C_2 amine groups protected and its use in copper (II) removal. *Water Science and Technology*, *76*(8), 2095-2105. http://dx.doi.org/10.2166/wst.2017.377

[21]. Fernando, M. S., Wimalasiri, A. K. D. V. K., Dziemidowicz, K., Williams, G. R., Koswattage, K. R., Dissanayake, D. P., De Silva, K. M. N., & De Silva, R. M. (2021). Biopolymer-based nanohydroxyapatite composites for the removal of fluoride, lead, cadmium, and arsenic from water. *ACS Omega*, *6*(12), 8517-8530. https://doi.org/10.1021/acsomega.1c00316

[22]. Gai, W., & Deng, Z. (2021). A comprehensive review of adsorbents for fluoride removal from water: performance, water quality assessment and mechanisms. *Environmental Science: Water Research & Technology*, *7*(8), 1362–1386. https://doi.org/10.1039/D1EW00232E

[23]. Garba, Z. N., Zhou, W., Lawan, I., Xiao, W., Zhang, M., Wang, L., Chen, L., & Yuan, Z. (2019). An overview of chlorophenols as contaminants and their removal from wastewater by adsorption: A review. *Journal of Environmental Management*, *241*, 59-75. https://doi.org/10.1016/j.jenvman.2019.04.004

[24]. Girkar, M., Shukla, S.P., Bharti, V., Kumar, K., & Bhuvaneswari, G.R. (2024). Removal of fluoride from ground water by chemically functionalized sugarcane bagasse bio char and bagasse pellets in a fixed-bed sorption system. *Desalination and Water Treatment*, *317*. 1-6. https://doi.org/10.1016/j.dwt.2024.100044

[25]. Goswami, R., & Kumar, M. (2018). Removal of fluoride from aqueous solution using nanoscale rice husk biochar. *Groundwater for Sustainable Development*, *7*, 446-451. https://doi.org/10.1016/j.gsd.2017.12.010

[26]. Grzegorzek, M., Majewwska-Nowak, K., & Ahmed, A. (2020). Removal of fluoride from multicomponent water solutions with the use monovalent selective ion exchange membranes. *Science of the total environment*, *722*, 137681. https://doi.org/10.1016/j.scitotenv.2020.137681

[27]. Hegde, R.M., Rego, R.M., Potla, K.M, Kurkuri, M.D., & Kigga, M. (2020). Bio-inspired materials for defluoridation of water: A review. *Chemosphere*, *253*, 1-20. https://doi.org/10.1016/j.chemosphere.2020.126657

[28]. Huang, R., Yang, B., Liu, Q., & Ding, K. (2012). Removal of fluoride ions from aqueous solutions using protonated cross-linked chitosan particles. *Journal of Fluorine Chemistry*, *141*, 29–34. https://doi.org/10.1016/j.jfluchem.2012.05.022

[29]. Isam, N., Dmour, I., & Taha, M.O. (2019). Degradability of chitosan micro/nanoparticles for pulmonary drug derivery. *Heliyon*, *5*(5), 1-9. https://doi.org/10.1016/j.heliyon.2019.e01684

[30]. Iwar, R. T., Ogedengbe, K. O., & Ugwudike, B. O. (2022). Groundwater fluoride removal by novel activated/aluminium oxide composite derived from raffia palm shells: Optimization of batch operations and field-scale point of use system evaluation. *Results in Engineering*, *14*, 1–12. https://doi.org/10.1016/j.rineng.2022.100407

[31]. Jagtap, S., Yenkie, M., Das, S., & Rayalu, S. (2011). Synthesis and characterization of lanthanum impregnated chitosan flakes for fluoride removal in water. *Desalination*, *273*(2), 267-275. https://ui.adsabs.harvard.edu/link_gateway/2011Desal.273..267J/doi:10.1016/j.desal.2010.12.032

[32]. Jaldurgam, F. F., Ahmad, Z. & Touati, F. (2021). Synthesis and performance of large-scale cost-effective environment-friendly nanostructured thermoelectric materials. *Nanomaterials*, *11*(5), 1091. https://doi.org/10.3390/nano11051091

[33]. Jawad, A. H., Mubarak, N. S. A., & Sabar, S. (2019). Adsorption and mechanism study for reactive red 120 dye removal by cross-linked chitosan-epichlorohydrin biobeads. *Desalination and Water Treatment*, *164*, 378–387. https://doi.org/10.5004/dwt.2019.24438

[34]. Johnston, N. R., & Strobel, S. A. (2020). Principles of fluoride toxicity and the cellular response: A review. *Archives of Toxicology, 94*(4), 1051–1069. https://doi.org/10.1007/s00204-020-02687-5

[35]. Kang, D., Yu, X., & Ge, M. (2017). Morphology-dependent properties and adsorption performance of CeO_2 for fluoride removal. *Chemical Engineering Journal*, *330*, 36–43. https://doi.org/10.1016/j.cej.2017.07.140

[36]. Kaszuba, M., Corbett, J., Watson, F.M., & Jone, A. (2010). High concentration zeta potential measurements using light- scattering techniques. *Philosophical Transactions of the Royal Society A: Mathematical, Physical and Engineering Sciences*, *368*, 4439-4451. https://doi.org/10.1098/rsta.2010.0175

[37]. Khan, A., Chen, Z., Zhao, S., Ni, H., Pei, Y., Xu, R., Ling, Z., Salama, E., Liu, P., & Li, X. (2017). Micro-aeration in anode chamber promotes *p*-nitrophenol degradation and electricity generation in microbial fuel cell. *Bioresource Technology, 285*, 1-31. https://doi.org/10.1016/j.biortech.2019.03.130

[38]. Khan, S. A., Khan, S. B., Khan, L. U., & Farooq, A. (2018). Fourier transform infrared spectroscopy: Fundamentals and application in functional groups and nanomaterials characterization. In S. Sharma (Ed.), *Handbook of Materials Characterization* (pp. 317–344). Springer International Publishing. https://doi.org/10.1007/978-3-319-92955-2_9

[39]. Kim, H., Cha, B., Nam, S., Yoon, Y., Hong, H., Elanchezhiyan, S.S., & Park, C.M. (2025). Synthesis of zirconium-based metal organic framework/gelatin aerogel for removing phosphate and fluoride from aqueous solutions. *International Journal of Biological Macromolecules*, *297*, 139749. https://doi.org/10.1016/j.ijbiomac.2025.139749

[40]. Kim, M., Choong, C.E., Hyun, S., Par, C.M., & Lee, G. (2020). Mechanism of simultaneous removal of aluminium and fluoride from aqueous solution by La/Mg/Si-activated carbon. *Chemosphere*, *253*, 126580. https://doi.org/10.1016/j.chemosphere.2020.126580

[41]. Kotrbova, A., Stepka, K., Maska, M., Palenik, J., Ilkovics, L., Klemova, D., Kravec, M., Hubotka, F.,Dave, Z., Hampl, A., Bryja, V., Matula, P., & Pospichalova, V.(2019). Tem Exosomer Analyzer: A computer-assisted software tool for quantitative evaluation of extracellular vesicles in transmission electron microscopy images. *Journal of Extracellular Vesicles, 8*(1), 1-13. https://doi.org/10.1080/20013078.2018.1560808

[42]. Krishna, D. N. G., & Philip, J. (2022). Review on surface-characterization applications of X-ray photoelectron spectroscopy (XPS): Recent developments and challenges. *Applied Surface Science Advances*, *12*, 100332. https://doi.org/10.1016/j.apsadv.2022.100332

[43]. Kurki, L., Oinonen, N., & Foster, A. (2024). Automated structure discovery for scanning tunneling microscopy. *ACSNano*, *18*(17), 11130-11138. https://doi.org/10.1021/acsnano.3c12654

[44]. Li, J., Li, B., Yu, W., Huang, H., Han, J., Huang, Y., Wu, X., Young, B., & Wang, G. (2022). Lanthanum-based adsorbents for phosphate reutilization: interference factors, adsorbent regeneration and research gaps. *Sustainable Horizons*, *1*, 100011. https://doi.org/10.1016/j.horiz.2022.100011

[45]. Li, X., Guo, Y.,Xie, Y. and Sun, Y. (2022). Treatment of fluoridated water with chitosan modified activated sludge lysis ash. *RCS Advances*, *12*(52), 34006-34019. https://doi.org/10.1039/d2ra05343h

[46]. Liu, R., Gong, W., Lan, H., Gao, Y., Liu, H., & Qu, J. (2011). Defluoridation by freshly prepared aluminum hydroxides. *Chemical Engineering Journal*, *175*(1), 144–149. https://doi.org/10.1016/j.cej.2011.09.083

[47]. Loganathan, K., & Ahamed, A. J. (2017). Multivariate statistical techniques for the evaluation of groundwater quality of Amaravathi River Basin: South India. *Applied Water Science*, *7*(8), 4633–4649. https://doi.org/10.1007/s13201-017-0627-0

[48]. Mandera-Santana, T.J., Mendez, C.H., & Rodriguez,, J.R. (2018). An overview of the chemical modification of chitosan and their advantages. *Green Materials*, *6*(4), 1-45. https://doi.org/10.1680/jgrma.18.00053

[49]. Mashale, K., Mogashane, T., Madzivha, P., Motlatle, M., Mokoena, L., & Tshilongo, J. (2025). Iron oxide and hydroxides for the removal of heavy metals from wastewater. In G. Montes-Atenas (Ed.), *Current research on mineralogy-minerals characterization and their applications*. IntechOpen. http://doi.org/10.5772/intechopen.1010016

[50]. Mawira, K.A., Nthiga, E.W., & Muthakia, G.K. (2023). Efficacy of quaternary ammonium functionalized waste paper bio-coagulant for removal of fluoride ions from aqueous solution. *International Journal of Scientific Research in Chemical Sciences*, *10*(2), 29-37. https://ijsrcs.isroset.org/index.php/j/article/view/130/130

[51]. Mayeen, A., Shaji, L. K., Nair, A. K., & Kalarikkal, N. (2018). Morphological characterization of nanomaterials. In N. Kalarikkal & A. K. Nair (Eds.), *Characterization of nanomaterials* (pp. 335–364). Elsevier. https://doi.org/10.1016/B978-0-08-101973-3.00012-2

[52]. Miretzky, P., & Cirelli, A.F. (2011). Fluoride removal from water by chitosan derivatives and composites: A review. *Journal of Fluorine Chemistry*, *132*(4), 231–240. https://doi.org/10.1016/j.jfluchem.2011.02.001

[53]. Mutalib, M. I. A., Rahman, M. A., Othman, M. H. D., Ismail, A. F., & Jaafar, F. (2017). Scanning electron microscopy (SEM) and energy dispersive X-ray (EDX) spectroscopy. In A. F. Ismail, M. H. D. Othman, & M. A. Rahman (Eds.), *Membrane characterization* (pp. 161-179). Penerbit UTM Press. https://doi.org/10.1016/B978-0-444-63776-5.00009-7

[54]. Mwangi, I., Mbugua, G., Wanjau, R., Sauda, S., Msagati, T., & Ngila, J. (2019). Removal of fluoride ions in stored drinking water by triethylamine chemically modified polyethylene containers. *International Journal of Environmental Research*, *13*(1), 175-184. https://doi.org/10.1007/s41742-018-0163-2

[55]. Nagaraj, V., & Kumar, B.M. (2018). Removal of fluoride from synthetic water using chitosan as an adsorbent. *IOSR Journal of Environmental Science, Toxicology and Food Technology (IOSR-JESTFT), 12*(4), 43-48. https://www.iosrjournals.org/iosr-jestft/papers/Vol12-%20Issue%204/Version-2/D1204024348.pdf

[56]. Ndiritu, J., Mwangi, I.W., Murungi, J.I., & Wanjau, R.N. (2020). Uptake of p-Nitrophenol(PNP) from model aqueous solutions using raw and quaternised Afromomum Malegueta peels. *African Journal of Pure and Applied Sciences*, *1*(1), 1-8. https://doi.org/10.33886/ajpas.v1i1.165

[57]. Nocella, G., Gutirrez, L., Akuno, M.H, Ghiglieri, G., Idini, A., &Carletti, A. (2022). Insights to promote safe drinking water behavioural changes in zones affected by fluorosis in East African Rift Valley. *GroundWater for Sustainable Development*; *19*: 100809. https://doi.org/10.1016/j.gsd.2022.100809

[58]. Othmani, A., Maitlo, H.A., & Hamimed, S. (2023). Chapter 3-Factors affecting adsorption capabilities of nanoscale materials. In *Micro and Nano Technologies, Adsorption through Advanced Nanomaterials, Elsevier*, pp 47-64. https://doi.org/10.1016/B978-0-443-18456-7.00003-1

[59]. Panhwar, S., Keerio, H., Khokhar, N., Muqueet, M., Ali, Z., Bilal, M., & Rehman, A. (2023). Magnetic nanomaterials as an effective absorbent material for removal of fluoride concentration in water: A review. *Journal of Water and Health*, *22*(1), 123-137. https://doi.org/10.2166/wh.2023.116

[60]. Patel, S., Han, J., Qiu, W., & Gao, W. (2015). Synthesis and characterisation of mesoporous bone char obtained by pyrolysis of animal bones, for environmental application. *Journal of Environmental Chemical Engineering*, *3*(4), 2368-2377. Article 746. https://doi.org/10.1016/j.jece.2015.07.031

[61]. Pathak, K., Misra, S., Sehgal, A., Singh, S., Bungau, S., Njda, A., Gruszeecki, R., & Behl, T. (2021). Biomedical applications of quaternised chitosan. *Polymers*, *13*(15), 2514. https://doi.org/10.3390/polym13152514

[62]. Patnaik,S., Mishra, P.C, Nayak, R.N., & Giri, A. (2016). Removal of fluoride from aqueous solution using chitosan iron complex. *Journal of Analytical and Bioanalytical Techniques*, *7*,326. doi:10.4172/2155-9872.100032

[63]. Perumal, S., Atchudan, R., Yoon, D., Joo, J. and Cheong, I. (2019). Spherical chitosan/gelatin hydrogel particles for removal of multiple heavy metal ions from waste water. *Industrial and Engineering Chemistry Research*, *58*(23):9900-9907. https://doi.org/10.1021/acs.iecr.9b01298

[64]. Pomari, A. A., Montanheiro, T. L., Siqueira, C. P., Silva, R. S., Tada, D. B., & Lemes, A. P. (2019). Chitosan hydrogels crosslinked by genipin and reinforced with cellulose nanocrystals: Production and characterization. *Journal of Composites Science*, *3*(3), 84–96. https://doi.org/10.3390/jcs3030084

[65]. Raghav, S., Nehra, S., & Kumar, D. (2019). Biopolymer scaffold of pectin and alginate for the application of health hazardous fluoride removal studies by equilibrium adsorption, kinetics and thermodynamics. *Journal of Molecular Liquids*, *284*, 203-214. https://doi.org/10.1016/j.molliq.2019.03.155

[66]. Rather, J., Akter, N., Ashraf, Q., Mir, S., Makroo, H., Majid, D., Barba, F.J., Khaneghah, A., Dar, B. (2022). A comprehensive review on gelatin: understanding impact of sources, extraction methods and modifications of potential packaging applications. *Food Packaging and Shelf Life*, *34*, 100945. https://doi.org/10.1016/j.fpsl.2022.100945

[67]. Robayo-Armortegui, H., Quintero-Attare, A., Florez-Navas, C., Serna-Palacious, I., Suarez-Saavedra, A., Buitrago-Bernal, R., & Casallas-Barrera, S. (2024). Fluid dynamics of life: exploring the physiology and importance of water in the critical illness. *Frontiers in Medicine*; *11*: 1368502. https://doi.org/10.3389/fmed.2024.1368502

[68]. Rojas-Mayorga, C., Bonilla-Petriciolet, A., Silvestre-Albero, J., Aguayo-Villarreal, I., & Mendoza-Castillo, D. (2015). Physico-chemical characterization of metal-doped bone chars and their adsorption behavior for water defluoridation. *Applied Surface Science*, *355*, 748–760. https://doi.org/10.1016/j.apsusc.2015.07.163

[69]. Rusiniak, P., Sekula, K., Sracek, O., & Stopa, P. (2021). Flouride ions in ground water of the Turkana County, Kenya, East Africa. *Acta Geochimica, 40*(6), 945-960. https://doi.org/10.1007/s11631-021-00481-3

[70]. Santhi, V., Periasamy, D., Perumal, M., Sekar, P., Varatharajan, V., Aravind, K., Senthikumar, K., Kumaran, S., Ali, S., Sankar, S., Vijayakumar, N., Boominathan, C., & Krishnan, R. (2024). The global challenge of fluoride contamination: A comprehensive review of removal processes and implications for human health and ecosystems. *Sustainability*, *16* (24), 11056. https://doi.org/10.3390/su162411056

[71]. Sarma, G., Sharma, R., Saikia, R.,Borgohain, X., Irakui, S., Bhattacharyya, K., & Rashid, M. (2020). Facile synthesis of chitosan ZnO/$ZnFe_2O_4$ nanocomposites for effective

remediation of ground water fluoride. *Environmental Science Pollution Research*, *27*(24), 30067-30080. https://doi.org/10.1007/s11356-020-09270-6

[72]. Senewirathna, D., Thuraisingam,S., Prabagar, S., & Prabaga, J. (2022). Fluoride removal in drinking water using activated carbon prepared from palmyrah (*Borassus flabellifer*) nut shells. *Current Research in Green Sustainable Chemistry*, *5*, 100304. https://doi.org/10.1016/j.crgsc.2022.100304

[73]. Shaumbwa,V., Liu, D., Archer, B., Li, J., & Su, F. (2021). Preparation and application of magnetic chitosan in environmental remediation and other fields-A review. *Journal of Applied Polymers*, *138*(42), e51241. https://doi.org/10.1002/app.51241

[74]. Silvestre, J., Delattre, C., Michaud, P. and Baynast, H. (2021). Optimization of chitosan properties with the aim of a water resistant adhesive development. *Polymers*, *13*(22), 4031. https://doi.org/10.3390/polym13224031

[75]. Siraj, K., & Kitte, S. (2023). Analysis of copper, zinc and lead using Atomic Absorption Spectrophotometer in groundwater of Jimma town of southern Ethiopia. *International Journal of Chemical and Analytical Science*, *4*(4), 201-204. https://doi.org/10.1016/j.ijcas.2013.07.006

[76]. Sultana, M., Ahmmed, M. R., Hoque, M. I. U., Mohsen, T. E., Mondal, A., Rahaman, M. H., Yesmin, M., Rahman, M. S., & Alam, S. M. N. (2023). Biodegradable composite of gelatin blend microcrystalline cellulose for Cd^{2+}, Pb^{2+}, and Cr^{3+} adsorption from an aqueous solution. *Advances in Polymer Technology*, *2023(1)*, 1–17. https://doi.org/10.1155/2023/1893660

[77]. Sun, Y., Zhang, C., Ma, J., Sun, W., & Shah, K. J. (2023). Review of fluoride removal technology from wastewater environment. *Desalination and water treatment*, *299*, 90-101. https://doi.org/10.5004/dwt.2023.29668

[78]. Sundaram, C., Viswanathan, N., & Meenakshi, S. (2009). Defluoridation of water using magnesia/chitosan composite. *Journal of Hazardous Materials*, *163*(2-3), 618–624. https://doi.org/10.1016/j.jhazmat.2008.07.009

[79]. Swain, S., Dey, R., Islam, M., Patel, R., Jha, U., Patnaik, T., & Airoldi, C. (2009). Removal of fluoride from aqueous solution using aluminium-impregnated chitosan biopolymer. *Separation Science and Technology*, *44*(9), 2096-2116. https://doi.org/10.1080/01496390902881212

[80]. Tan, Y., Davis, J., Fujikawa, K., Ganesh, N., Demchenko, A. and Stine, K. (2012). Surface area and pore size characteristics of nanoporous gold subjected to thermal, mechanical or surface modification studied using gas adsorption isotherms, cyclic voltammetry, thermogravimetric analysis and scanning electron microscopy, *22*(14), 6733-6745. https://doi.org/10.1039/C2JM16633J

[81]. Tandon, R., Tandon, N., Gupta, N., & Gupta, R. (2017). Art of synthesis of desired polymorphs: A review. *Asian Journal of chemistry*, *30*(1), 5-14. https://doi.org/10.14233/ajchem.2018.20934

[82]. Tazik, M., Dehghani, M. H., Yaghmaeian, K., Nazmara, S., Salari, M., Mahvi, A. H., Nasseri, S., Soleimani, H., & Karri, R. R. (2023). 4-chlorophenol adsorption from waste water solutions by activated carbon functionalized with amine groups: response surface method and artificial neural networks. *Scientific Reports*, *13*(1), 7831–7839. https://doi.org/10.1038/s41598-023-35117-4

[83]. Tillet, G., Boutevin, B., & Améduri, B. (2011). Chemical reactions of polymer crosslinking and post-crosslinking at room and medium temperature. *Progress in Polymer Science*, *36*(2), 191–217. https://doi.org/10.1016/j.progpolymsci.2010.08.003

[84]. Tolkou, A. K., Posantzis, A., Maroulas, K. N., Kosheleva, R. I., Koumentakou, I., Kostoglou, M., & Kyzas, G. Z. (2024). Fluoride removal from aqueous solutions by using super-adsorbents of chitosan/orange peels/activated carbon@MgO: Synthesis, characterization, and adsorption evaluation. *Processes*, *12*(9), 2043. https://doi.org/10.3390/pr12092043

[85]. Valdez-Alegria, C., Fuentes-Rivas, R., Garcia-Rivas, J., Arce, R., Nunez, M., & Garcia-Gaitan, B. (2020). Synthesis of chitosan-polyvinyl alcohol biopolymers to eliminate fluorides from water. *Biomolecules*, *10*(1), 156. https://doi.org/10.3390/biom10010156

[86]. Vijaya, Y., Popuri, S. R., Reddy, A. S., & Krishnaiah, A. (2011). Synthesis and characterization of glutaraldehyde crosslinked calcium alginate for fluoride removal from aqueous solutions. *Journal of Applied Polymer Science*, *120*(6), 3443–3452. https://doi.org/10.1002/app.33375

[87]. Viswanathan, N., Sundaram, C., & Meenakshi, S. (2009). Sorption behaviour of fluoride on carboxylated cross-linked chitosan beads. Colloids and Surfaces B: *Biointerfaces*, *68*(1), 48–54. https://doi.org/10.1016/j.colsurfb.2008.09.009

[88]. Wei, Y., Wang, L., Li, H., Yan, W. and Feng, J. (2022). Synergistic fluoride adsorption by composite adsorbents synthesized from different type of materials-A review. *Frontiers in Chemistry*; 10, Article 900660. https://doi.org/10.3389/fchem.2022.900660

[89]. Yammine, P., Safadi, A., Kassab, R., El-Nakat, H., Obeid, P., Nasr, Z., Tannous, T., Sari-Chmayssem, N., Mansour, A., & Chmayssem, A. (2025). Types of crosslinkers and their applications in biomaterials and biomembranes. *Chemistry*, *7*(2), 61. https://doi.org/10.3390/chemistry7020061

[90]. Yang, B., Sun, G., Quan, B., Tang, J., Zhang, C., Jia, C., Tang, Y., Wang, X., Zhao, M., Wang, W., & Xiao, B. (2021). An experimented study of fluoride removal from wastewater by Mn-Ti-modified zeolite. *Water*, *13*(23), 3343. https://doi.org/10.3390/w13233343.

[91]. Yang, W., Shi, F., Jiang, W., Chen, Y., Zhang, K., Jian, S., Jiang, S., Zhang, C., & Hu, J. (2022). Outstanding fluoride removal from aqueous solution by a lanthanum-based adsorbent. *Royal Society of Chemistry Advances*, *12*, 30522-30528. https://doi.org/10.1039/D2RA06284D

[92]. Yang, Z., & Freund, H.-J. (2024). High-speed scanning tunneling microscope technique and its application in studying structural dynamics on surfaces**.** *Progress in Surface Science***,** *99*(2), 100744**.** https://doi.org/10.1016/j.progsurf.2024.100744

[93]. Yang, Z., & Yuan, Y. (2001). Studies on the synthesis and properties of hydroxyl Azacrown ether-grafted chitosan. *Journal of Applied Polymer Science*, *82*(8), 1838-1843. https://doi.org/10.1002/app.2026

[94]. Yu, Y., Chen, C., Dhanasinghe, C., Verpoort, F., Surampalli, S., Chen, S., & Kao, C. (2024). Development of modified MgO/ biochar composite for chemical adsorption enhancement to clean up fluoride–contaminated groundwater. *Journal of Environmental Management*, 370, 123016. https://doi.org/10.1016/j.jenvman.2024.123016

[95]. Zeng, X. and Ruckenstein, E. (1998). Crosslinked macroporous chitosan anion-exchange membrane for protein separations. *Journal of Membrane Science*, *148* (2), 195-205. https://doi.org/10.1016/S0376-7388(98)00183-5

[96]. Zhang, Y., Zhang, W., Shen, S., Yan, X., Wu, R., Wu, A., Lastoskie, C., & Zhang, J. (2017). Sacrificial template strategy toward a hollow $LiNi_{1/3}Co_{1/3}Mn_{1/3}O_2$ nanosphere cathode for advanced lithium ion batteries. *ACS Omega*, *2*(11), 7593-7599. https://doi.org/10.1021/acsomega.7b00764

[97]. Zhao, D., Yang, Y., & Chen, J. (2024). Performance of removing aqueous contaminant by zirconium based adsorbents: A critical review. *Frontiers of Chemical Engineering*, *6*, 1282076. https://doi.org/10.3389/fceng.2024.1282076

[98]. Zhou, N., Guo, X., Xe, C., Yan, L., Gu, W., Wu, X., Zhou, Y., Wang, X., & Cheng, Q. (2021). Enhanced fluoride removal from drinking water in wide pH range using La/Fe/Al oxides loaded rice straw bio char. *Water Supply*, *22*(1),779-794. https://doi.org/10.2166/ws.2021.232

[99]. Zhou, Y., Yu, C., & Shan, Y. (2004). Adsorption of fluoride from aqueous solution on La^{3+}-impregnated cross-linked gelatin. *Separation and Purification Technology*, *36*(2), 89-94. https://doi.org/10.1016/S1383-5866(03)00167-9

[100]. Zielińska, A., Carreiró, F., Oliveira, A. M., Neves, A., Pires, B., Venkatesh, D. N., Durazzo, A., Lucarini, M., Eder, P., Silva, A. M., Santini, A., & Souto, E. B. **(**2020**).** Polymeric nanoparticles: Production, characterization, toxicology and ecotoxicology. *Molecules***,** *25*(16), 3731. https://doi.org/10.3390/molecules25163731

[101]. Žigrayová, D., Mikušová, V., & Mikuš, P. (2024). Advances in chitosan derivatives: Preparation, properties and applications in pharmacy and medicine. *Gels*, *10*(11), 701-702. https://doi.org/10.3390/gels10110701

[102]. Zúñiga-Muro, N. M., Bonilla-Petriciolet, A., Mendoza-Castillo, D. I., Reynel-Ávila, H. E., & Tapia-Picazo, J. C. (2017). Fluoride adsorption properties of cerium-containing bone char. *Journal of Fluorine Chemistry*, *197*, 63–73. https://doi.org/10.1016/j.jfluchem.2017.03.004